Two-Dimensional Nitrides as Highly Efficient Potential Candidates for CO_2 Capture and Activation†

Raul Morales-Salvador, Ángel Morales-García, Francesc Viñes, Francesc Illas*

Departament de Ciència de Materials i Química Física & Institut de Química Teòrica i Computacional (IQTCUB), Universitat de Barcelona. c/ Martí i Franquès 1, 08028 Barcelona, Spain

Abstract

The performance of novel two-dimensional nitrides in carbon capture and storage (CCS) is analyzed for a broad range of pressure and temperature conditions. Employing an integrated theoretical framework where CO_2 adsorption/desorption rates on the M_2N (M= Ti, Zr, Hf, V, Nb, Ta, Cr, Mo, W) surface are derived from transition state theory and density functional theory based calculations, the present theoretical simulations consistently predict that, depending on the particular composition, CO_2 can be strongly adsorbed and even activated at temperatures above 1000 K. For practical purposes, Ti_2N, Zr_2N, Hf_2N, V_2N, Nb_2N, Ta_2N are predicted as the best suited materials for CO_2 activation. Moreover, the estimated CO_2 uptake of 2.32–7.96 mol $CO_2 \cdot kg^{-1}$ reinforces the potential of these materials for CO_2 abatement.

E-mail: francesc.illas@ub.edu; Fax: +34-93-402-1231; Tel: +34-93-402-1229

† Electronic supplementary information (ESI) available: See DOI:

Introduction

There is no doubt that the continued increase in the concentration of CO_2 in the Earth atmosphere directly correlates with global warming and that, in turn, such increase is strongly related to anthropogenic emissions resulting from the use of fossil fuels.[1] The need to reduce the amount of this greenhouse gas has triggered research into CO_2 sequestration with the idea not only to contribute decreasing its concentration in the atmosphere[2,3] but of its ulterior utilization as a chemical feedstock in the chemical industry. This may look as a simple idea but its practical implementation into a sufficiently large scale constitutes an enormous scientific and technological challenge.[4] This is because of the very high stability of gas phase CO_2, the final product of spontaneous combustion of fuels based on organic compounds such as wood, natural gas, or gasoline.

The high chemical stability of CO_2 also implies weak interaction with solid substrates, which, according to the well-known Sabatier principle, encounters problems when aiming at using heterogeneous catalysts for CO_2 conversion. Hence, in the absence of sufficiently active catalysts, CO_2 capture appears as more attractive than direct conversion. Indeed, CO_2 capture based on amine-scrubbing technology has become a widely used method.[5,6] Nevertheless, because of its non-corrosive nature, low-cost, and easy regeneration, capture by solid materials is considered as advantageous.[7,8] The use of solid materials is the basis for the so-called carbon capture and storage (CCS) strategy. The requirements are similar yet less stringent than for heterogeneous catalytic conversion.[9] In fact, CCS requires a specific type of solid-substrate able to adsorb CO_2 in a sufficient strong way. Ideally, one would like to have materials able to trigger activation usually involving charge transfer towards the molecule resulting in the generation of bent anionic $CO_2^{\delta-}$ species. This is the case for CO_2 sequestration through carbonation of natural silicate minerals driving to the formation of carbonates. Unfortunately, this fixes CO_2 to the substrate making it unavailable for subsequent conversion.[10,11] In order to find appropriate candidates for CCS, a large number of diverse materials has been analysed involving metals, metal oxides, graphene-based materials, zeolites, metal-organic frameworks and transition metal carbides[12-19] although with not completely satisfactory results.

The preceding discussion clearly illustrates the need to go beyond existing materials and to look for alternatives. In this sense, it is worth mentioning that an entirely new family of two-dimensional (2D) transition metal carbides and nitrides has been reported quite recently. These materials have a general $M_{n+1}X_n$ chemical formula where M stands for early transition metals and X for C or N.[20,21] Depending on n, which runs from 1 to 3, the resulting materials have 3, 5, or 7 atomic layers. Because of the similarities with graphene, including a hexagonal atomic structure, this new materials have been designed as MXenes. At present, several members of the potentially very large MXene family have been synthesized from the precursor so-called MAX phases.[22] This was initially achieved by selectively etching Al from Ti_3AlC_2 and other Al-containing MAX phases using hydrogen fluoride.[23] However, the progress in this field is very fast and fluorine-free synthetic procedures have recently been proposed to synthesize MXenes.[24,25] Even, more

recently, MXene synthesis from other MAX phases not containing Al has been achieved[26] which shows that the number of these materials already obtained is likely to represent a small fraction of those to be obtained in the near future.

Among other properties recently reviewed,[20,26] MXenes display high surface areas up to 1000 $m^2 g^{-1}$ and excellent stability.[23] The high surface area displayed by MXenes together to the reactivity of transition metal carbides towards CO_2 adsorption and activation[18] triggered a systematic research where the CCS ability of MXenes with M_2C formula have been computationally investigated.[27] Using adsorption and desorption rates derived from transition state theory and density functional theory based calculations, it has been shown that the M_2C MXenes are able to adsorb and release CO_2 at rather high temperatures and low partial pressures. Moreover, CO_2 uptakes ranging from 2.34 to 8.25 mol CO_2 kg^{-1} of substrate have been predicted which are a direct consequence of their chemical activity and high surface area. It is worth pointing out that this uptake is equivalent to that of other porous material used regularly for CCS purposes such as zeolites,[28,29] derivatives of graphene,[30] or bulk MgO nanopowders[31].

In the view of the very large number of potential MXene compounds and motivated by the encouraging results obtained for the M_2C subset,[27] we analyse the CCS capabilities of the M_2N (M= Ti, Zr, Hf, V, Nb, Ta, Cr, Mo, W) family for which information is scarce and new and fascinating chemistry is likely to emerge. In fact, just from the higher electronic conductivity one can already expect that their overall chemistry would be significantly different from that of their carbide counterparts. Moreover, the fact that Ti_2N has been already obtained and characterized[32] can be seen as a starting point in the development of efficient synthetic routes leading to other members of the M_2N family.

Materials models and computational methods

Models

Surface slabs models were used to represent the basal (0001) plan of the M_2N materials studied in the present work. The models were built using the crystal structure of the corresponding precursor MAX phase by removing the A element and re-optimizing both lattice parameter and fractional coordinates. The resulting slabs have three atomic layers featuring a M-N-M sandwich-like configuration as schematically shown in Fig. 1. In order to avoid interaction between the adsorbed CO_2 molecules in the periodically replicated images a $p(3\times3)$ supercell was used containing 18 M and 9 N atoms. Also, since the computational code used (see below) exploits periodic symmetry in the three directions it is necessary to add a vacuum region to avoid the interaction between interleaved slabs; a vacuum width of 10 Å probed to be sufficient to obtain numerically converged results.

Density Functional Theory based calculations

The interaction of CO_2 with the $M_2N(0001)$ surfaces is studied by means of density functional theory (DFT)[33,34] based calculations within the PBE implementation of the generalized gradient approximation

(GGA) for the exchange-correlation potential.[35] Additionally, the contribution of dispersion terms to the interaction of CO_2 with the $M_2N(0001)$ systems is taken into account through the D3 parameterization of the method proposed by Grimme.[36] To solve the corresponding Kohn-Sham equations, the valence electron density is expanded in a plane-wave basis set with a cutoff of 415 eV for the kinetic energy, a choice that leads to converged results up to 1 meV whereas the interaction between the valence electron density and the core electrons is accounted for through the projector augmented wave (PAW) method.[37] Integration in the reciprocal space is carried out using a 5×5×1 grid of Monkhorst-Pack special ***k***-points.[38] Convergence in the geometry optimization is reached when forces acting on nuclei are all below 0.01 eV/Å. The adsorption energy is defined as $E_{ads} = E_{CO_2/M_2N} - (E_{M_2N} + E_{CO_2}) + \Delta E_{ZPE}$, where E_{CO_2/M_2N} corresponds to the energy of CO_2 adsorbed on M_2N surface and E_{M_2N} stands for the energy of the relaxed pristine M_2N surface; E_{CO_2} corresponds to the energy of an isolated CO_2 molecule computed in a symmetric box of 10×10×10 Å dimensions and using the **Γ**-point only. Finally, ΔE_{ZPE} corresponds to difference in zero-point energy (ZPE) of each term contribution calculated in the harmonic approximation. Note that the vibrational frequencies were calculated decoupled form surface phonons and including frustrated rotations/translations. Attending to this definition of E_{ads}, adsorption is associated to negative values and the more negative the stronger the interaction is. All DFT based calculations are performed with the Vienna *ab initio* Simulation Package (VASP).[39,40]

Adsorption/Desorption Rates

Assuming that CO_2 adsorption is a non-activated process, a meaningful choice, the adsorption rate r_{ads} can be calculated from the well-known Herz-Knudsen formula as in Eq. (1),[18,41]

$$r_{\text{ads}} = \frac{S_0 \cdot p_{\text{CO}_2} \cdot A}{\sqrt{2\pi \cdot m \cdot k_B \cdot T}} \qquad (1),$$

where S_0 is the initial sticking coefficient, p_{CO_2} corresponds to the CO_2 partial pressure above the surface, A stands for the area of an active adsorption site and m corresponds to the mass of the adsorbed molecule. A conservative value of $S_0 = 0.40$ is selected for our study following a previous analysis where the CO_2 capture, storage and activation were investigated on transition metal carbides and two-dimensional M_2C MXenes.[18,27] Note that equal adsorption probability of all sites (Fig. 1) is assumed and therefore, A is approached as the supercell area of each surface divided by the total number of adsorption sites in it. Three different pressure values representative of different conditions of interest are selected to evaluate r_{ads}: *i*) the atmospheric partial pressure of CO_2, $p_{\text{CO}_2} = 40$ Pa;[42] *ii*) a partial pressure of $p_{\text{CO}_2} = 0.15$ bar ($15 \cdot 10^3$ Pa) which is a reference value for post-combustion exhaust gases;[43] *iii*) a partial pressure of $p_{\text{CO}_2} = 1.0$ bar (10^5 Pa) corresponding to a reference for pure CO_2 stream generation from a carbon capture and storage (CCS) system.[44]

The rate of desorption, r_{des}, has been estimated from transition state theory (TST)[45] stating that the reaction rate r_{i} of an elementary step is given by

$$r_{\mathrm{i}} = v \cdot exp\left(-\frac{\Delta E}{k_B \cdot T}\right); v = \frac{k_B \cdot T \; q\#}{h \cdot q_0} \quad (2),$$

where k_BT is the product of Boltzmann constant, k_B, and the temperature, T, and ΔE would be associated to the zero point corrected energy barrier for the described elementary step, here using the (negative) E_{ads} values implying that the transition state is supposed to be located infinitely close to the desorption final state. In Eq. (2), v is the well-known pre-exponential actor term also provided by TST with h, $q^{\#}$ and q_0 being the Planck constant, and partition functions of the transition and initial states, respectively. Hence one has

$$r_{\mathrm{des}} = v_{\mathrm{des}} \cdot exp\left(\frac{E_{\mathrm{ads}}}{k_B \cdot T}\right); \; v_{\mathrm{des}} = \frac{k_B \cdot T \cdot q_{trans,2D}^{gas} \cdot q_{rot}^{gas} \cdot q_{vib}^{gas}}{q_{vib}^{ads}} \quad (3),$$

where v_{des} contains the partition function of the molecule in an early 2D transition state in the numerator. This partition function is given by the product $q_{trans,2D}^{gas} \cdot q_{rot}^{gas} \cdot q_{vib}^{gas}$ in which $q_{trans,2D}^{gas}$ stands for the partition function for translational motion in two dimensions whereas, q_{rot}^{gas} and q_{vib}^{gas} correspond to the rotational and vibrational partition functions of the CO_2 molecule in the gas phase, respectively. Once the molecule is adsorbed on the surface all degrees of freedom are considered as vibrations since molecular translations and rotations become frustrated through interaction with the substrate and effectively converted into vibrations. The q_{vib}^{gas} partition function contains vibrational contributions only. Finally, note that the electronic partition function is set to 1, which is justified by the high energy of the excited electronic states. Therefore, the necessary partition functions were evaluated as

$$q_{trans,2D}^{gas} = A \cdot \frac{2\pi \cdot k_B \cdot T}{h^2} \quad (4),$$

$$q_{vib}^{ads/gas} = \prod_i \frac{exp\left(-\frac{h \cdot v_i}{2 \cdot k_B \cdot T}\right)}{1 - exp\left(-\frac{h \cdot v_i}{k_B \cdot T}\right)} \quad (5),$$

$$q_{rot}^{gas} = \frac{T}{2 \cdot T_{\mathrm{rot}}} \quad (6),$$

where v_{i} is the harmonic vibrational frequency of each normal mode as predicted from the present DFT based calculations, either for CO_2 molecule in vacuum or adsorbed, $2 \cdot T_{\mathrm{rot}}$ is the product of the rotational temperature for CO_2 and its symmetry number, 2. T_{rot} is taken from the literature as 0.561 K.[46]

Results and discussion

One of the main goals of the present study is to provide qualitative and quantitative information regarding the interaction— and possible activation— of CO_2 with $M_2N(0001)$ surfaces. To this end, a

systematic computational search has been launched considering different orientations of the CO_2 molecule with respect to the surface plane and taking all possible adsorption sites into account. The final atomic structure of the adsorbed CO_2 molecules predicted by the geometry optimization using an appropriate DFT based method reduces to eight particular sites and the explored M_2N systems display at least one of these configurations. To distinguish among these eight bonding modes a notation is used in which the first digit (n) is assigned depending on the number of atoms of the CO_2 molecule (1, 2, or 3) close enough to the surface (η^n-CO_2). Clearly, this depends on the orientation of the adsorbed CO_2 molecule as clearly seen in the side view in Fig. 1. The notation uses a second digit (m) describing the atomic environment (2, 3, 4, or 5) of the adsorbed CO_2 molecule (μ^m) and ends by a specification of the location of the n surface atoms in contact with the CO_2 molecule (N, M, or B which correspond to Nitrogen hollow, Metal hollow, or Bridge sites). Hence, the eight different bonding modes are univocally labelled as follow, η^1-CO_2-μ^2-C_B, η^2-CO_2-μ^3-C_MO_B, η^2-CO_2-μ^3-C_NO_B, η^3-CO_2-μ^5-$C_MO_NO_N$, η^3-CO_2-μ^5-$C_NO_MO_M$, η^2-CO_2-μ^3-O_BO_B, η^3-CO_2-μ^4-$C_BO_BO_B$, and η^3-CO_2-μ^4-$C_MO_MO_B$. Note also that whether a given bonding mode appears or not depends on each particular M_2N surface. For instance, O_BO_B and $C_MC_MO_B$ are only found in Ta_2N and W_2N. However, on most cases (Hf_2N, V_2N, Nb_2N, Ta_2N, Cr_2N, Mo_2N, and W_2N) C_B is the most favourable bonding mode for CO_2 adsorption. It is worth pointing out that this bonding mode was also found to be the second most favourable one for the interaction of CO_2 with the related M_2C series of MXenes.[27] Note, however, that structural features of the M_2N materials here studied lead to sites for CO_2 that are more accessible than those of their carbide counterparts.

The analysis of results in Table 1 shows that the PBE-D3 calculated adsorption energy (E_{ads}) values are quite large ranging from -1.03 (Mo_2N) to -3.13 eV (Ti_2N) indicating a very strong interaction. Interestingly, these values are only slightly smaller than those reported at the same computational level for their M_2C counterparts running from -1.13 to -3.69 eV.[27] This origin of this difference is quite simple to understand, the N layer in the M_2N systems withdraws more charge density from the metal layers than the C layer in the M_2C ones implying a reduction in the charge transfer from the metallic layer of the MXene towards CO_2. Table 1 also shows that E_{ads} generally decreases (less negative values indicate weaker adsorption) when moving along the *d* series, which is consistent with the trends reported for CO_2 adsorption on several M_3C_2 and M_2C systems.[18,27,47] One remarkable difference between M_2C and M_2N systems is the importance of the contribution of dispersion terms to E_{ads}. The inclusion of these terms through the D3 Grimme method increases the PBE calculated E_{ads} (in absolute terms) for M_2N materials by quite a significant amount (0.7–1.0 eV) where a smaller contribution of ~0.40 eV was found for the studied M_2C compounds. One could argue that the larger contribution for M_2N materials arises from artefacts in the empirical parameters entering in the D3 methods. To rule out this possibility, calculations have also been carried out with the better theoretically grounded Tkatchenko-Scheffler (TS)[48] or the more sophisticated surface many-body dispersion (MBD) approach[49]. For V_2N, the calculated D3 contribution to E_{ads} is -0.69

eV, in full agreement with values of -0.68 and -0.71 eV as predicted from TS and MBD methods, respectively (Additional details regarding these issues can be found in the ESI†). This unexpected important contribution of dispersion terms of up to 1 eV has significant implications in the temperature range at which CO_2 desorbs, which we discuss in more detail later. Here we note that, in spite of the strong interaction, the geometry optimization procedure always converges to some of the molecularly adsorbed states described above with no evidence of dissociative chemisorption indicating that this would take place an energy barrier would have to be overcome. Interestingly, a bent adsorbed CO_2 molecule is found in most cases with the O-C-O angle in the 111 to 137° range and the C-O bond distances in the 1.25-1.44 Å interval, significantly larger than the value for the isolated gas phase molecule. The chemical activation of adsorbed CO_2 is additionally confirmed by the net charged computed using the Bader atoms-in-molecules analysis[50] indicating the formation of highly anionic adsorbed $CO_2^{\delta-}$ species with charges running from -0.86 to -2.02 *e*. The results discussed so far support the claim that M_2N systems are appropriate for CO_2 activation.

The very large adsorption energy and concomitant activation of CO_2 on $M_2N(0001)$ surfaces strongly suggest that CO_2 may be adsorbed up to quite high temperatures. Making use of the above described theoretical framework r_{ads} and r_{des} rates are estimated for a broad range of temperatures as high as 2000 K. Although the upper limit corresponds to a very high temperature it is below the melting point of the corresponding 3D transition metal nitrides, ranging from 2350 to 3330 K.[51,52] Obviously, the adsorption rate has a non-negligible dependence with the number of CO_2 molecules hitting the surface and so on the CO_2 partial pressure (p_{CO_2}). Also, desorption rate is determined by the adsorption energy which in turn depends on the bonding mode (Table 1). Hence, two desorption curves for each M_2N have been built which differ on whether the PBE or PBE-D3 E_{ads} value is used. This choice allows one to consider the least and most favourable adsorption situations thus avoiding any bias from the choice of a given computational method and providing a reasonable range of values for subsequent analysis. The estimated r_{ads} and r_{des} are illustrated in Fig. 2a for M_2N systems with the lowest (Cr_2N) and highest (Ti_2N) E_{ads} values (see also Tables 1 and S1 in the Electronic supplementary information, ESI†). Note that two sites ($C_MO_NO_N$ and $C_NO_MO_M$) with similar adsorption strength are found for Ti_2N and, hence, only an estimated r_{des} including PBE and PBE-D3 is expected for this MXene as reported in Fig. 2a.

Let us now describe in detail the features of the plots of adsorption/desorption rates shown in Fig. 2a. The crossing point between r_{ads} and r_{des} indicates the dynamical equilibrium state where the adsorption and desorption rates coincide, temperatures below the crossing point favour adsorption and, consequently, CO_2 becomes sequestered at the material surface. For the case of Cr_2N at 40 Pa p_{CO_2} (labelled as air), two intersections at temperatures of 106 and 579 K are clearly seen corresponding to the weakest (PBE) and the strongest (PBE-D3) estimates, respectively. In this way, T_1-T_2 defines the temperature range below which CO_2 adsorption dominates and, consequently, it would become stored on the M_2N surface, above this temperature desorption will prevail and CO_2 will be released to the gas phase. Note that an increase of p_{CO_2}

to $15 \cdot 10^3$ Pa shifts these limits to the T_3-T_4 interval corresponding to higher values and this is even further increased at 1 bar pressure as indicated by the T_5-T_6 interval. Note that these temperature ranges are quite large for Cr_2N and W_2N and this is mainly due to the significant high contribution of dispersion terms (PBE-D3 value) to the adsorption energy value. The average adsorption/desorption switch temperature for the whole set of M_2N surfaces explored in the present work is ~1000 K (see Fig. 2b). Interestingly enough, this appears to be quite below the average value for their M_2C counterparts where this occurs at ~1250 K.[27]

The above discussion applies to every M_2N surface studied and the analysis of the rest of cases is summarized in Fig. 2b where the temperature ranges are shown, independent of the particular adsorption energy and rate. Further information is provided in Table S3 in the ESI† including details regarding the temperature range for each particular site of each M_2N surfaces. From Fig. 2b it also appears that M_2N materials with high adsorption energies feature elevated temperature ranges. Therefore, Ti_2N, Zr_2N, and Hf_2N (d^2 MXenes) display the largest temperature ranges, whereas Cr_2N, Mo_2N, and W_2N (d^4 MXenes) feature the smallest. The present results strongly suggest that, for practical purposes, d^2 and d^3 nitride MXenes (Ti_2N, Zr_2N, Hf_2N, V_2N, Nb_2N, and Ta_2N) are among the most appealing materials for CO_2 abatement. This is reinforced by the fact that adsorption/desorption transitions at air conditions are located near or within room temperature. Indeed, M_2N materials show a larger adaptability than M_2C counterparts, where only Mo_2C and W_2C met this criterion.

To further examine the capability of the M_2N materials to store CO_2 we focus in the total amount of this compound that can be stored CO_2 per kg of substrate and compare to the values for different families of materials that have been successfully proved such as Ca-X and 13X zeolites,[28,29] with 3.36 and 2.96 mol CO_2 kg^{-1}, respectively, or derivatives of graphene, *e.g.* a-RGO-950[30] with 3.36 mol CO_2 kg^{-1}, which are clearly better than using bulk MgO nanopowders,[32] with 0.92 mol CO_2 kg^{-1}. To model the potential amount of CO_2 storage by the M_2N materials we take into account the surface exposure and possible CO_2 loading to the high surface area exposed by 2D MXenes.[23] For the $p(3\times3)$ supercell model employed in this study, one can safely argue that each M_2N surface could simultaneously adsorbed four CO_2 molecules. From this quite a conservative estimate one readily predicts that the M_2N compounds studied in the present work would be able to adsorb 2.32–7.96 mol CO_2 kg^{-1} of substrate (Fig. 3). Clearly, practical operating conditions would require CO_2 separation from other competing (combustion) gases prior to adsorption, although recent studies on a series of 2D (MXenes) and 3D transition metal carbides show a high adsorption preference for CO_2 with respect to other gases such as CO or CH_4 by more than 1.5 eV.[53,54]

Conclusions

The computational modelling presented in this study, based on state of the art DFT based calculations and the use of transition state theory derived adsorption/desorption rates highlights the potential of the 2D M_2N materials (M = Ti, Zr, Hf, V, Nb, Ta, Cr, Mo, W) for CO_2 storage and activation. Our study reports high adsorption energies up to -3.13 eV accompanied by a noticeably large CO_2

activation, evidenced by the appearance of a strongly anionic $CO_2^{\delta-}$ adsorbed species with elongated δ(CO) bonds, bent structures, and significant MXene→CO_2 charge transfer. The high adsorption energies are remarkable since one must point out that CO_2 adsorbs very weakly on most materials. The significantly large adsorption energy value for CO_2 on the M_2N materials makes them even more suitable than their carbide (M_2C) counterparts indicating that M_2N materials may constitute effective alternatives for efficient CO_2 capture, storage, and activation. This is supported by the temperature ranges for adsorption/desorption switch and by predicted CO_2 uptakes ranging from 2.32 to 7.96 mol CO_2 kg^{-1} of substrate, quite competitive to other nowadays-existent material solutions. Finally, the fact CO_2 become highly activated suggest that these 2D M_2N MXenes could also constitute active catalysts for CO_2 conversion although this requires additional research. We hope the present results will stimulate further research in the synthesis of new members of the M_2N family as well as experimental studies regarding their CCS capability.

Conflicts of interest

There are no conflicts to declare

Acknowledgements

The authors acknowledge financial support from the Spanish *Ministerio de Economía y Competitividad* (MINECO) through the CTQ2015-64618-R grant which including FEDER funds. The authors wish also to thank *Generalitat de Catalunya* for partial support through 2017SGR13 and XRQTC grants and from the NOMAD Center of Excellence project; the latter received funding from the European Union´s Horizon 2020 research and innovation programme under grant agreement no. 676580. A. M.-G. and F. V. are indebted to MINECO for *Juan de la Cierva* (FJCI-2015-23760) and *Ramón y Cajal* (RYC-2012-10129) postdoctoral research contracts, respectively. F. I. acknowledges additional support from the 2015 ICREA Academia Award for Excellence in University Research.

Table 1 Zero point corrected PBE-D3 adsorption energies (E_{ads}) for CO_2 above different sites of the M_2N 0001) surfaces. PBE values and other further details are given in the ESI†. The coordination notation is denoted in parenthesis to diferenciate the adsorption sites shown in Fig. 1.

	MXene	E_{ads} (eV)		
d^2	Ti_2N	-3.13 ($C_MO_NO_N$)	-3.13 ($C_NO_MO_M$)	-
	Zr_2N	-2.97 ($C_MO_NO_N$)	-	-
	Hf_2N	-2.97 ($C_MO_NO_N$)	-2.29 (C_B)	-
d^3	V_2N	-1.67 (C_B)	-1.65 (C_MO_B)	-1.51 (C_NO_B)
	Nb_2N	-1.73 (C_B)	-1.69 (C_MO_B)	-1.50 (C_NO_B)
	Ta_2N	-1.90 (C_B)	-1.90 ($C_NO_MO_M$)	-0.61 (O_BO_B)
d^4	Cr_2N	-1.44 ($C_BO_BO_B$)	-1.30 (C_B)	-1.21 (C_NO_B)
	Mo_2N	-1.34 (C_B)	-1.34 ($C_BO_BO_B$)	-1.03 (C_MO_B)
	W_2N	-2.59 ($C_MO_MO_B$)	-1.77 ($C_NO_MO_M$)	-1.21 (C_B)

Fig. 1 Side and top view of models featuring CO_2 adsorbed on eight possible sites of M_2N (0001) surfaces. The colour sequence is as follows: brown and red spheres correspond to carbon and oxygen atoms of the CO_2 molecule; and dark and light blue spheres to M upper and bottom layers, respectively, whereas the inner nitrogen layer is represented by dark yellow spheres in the M_2N(0001) surface. The coordination notation is given below each site.

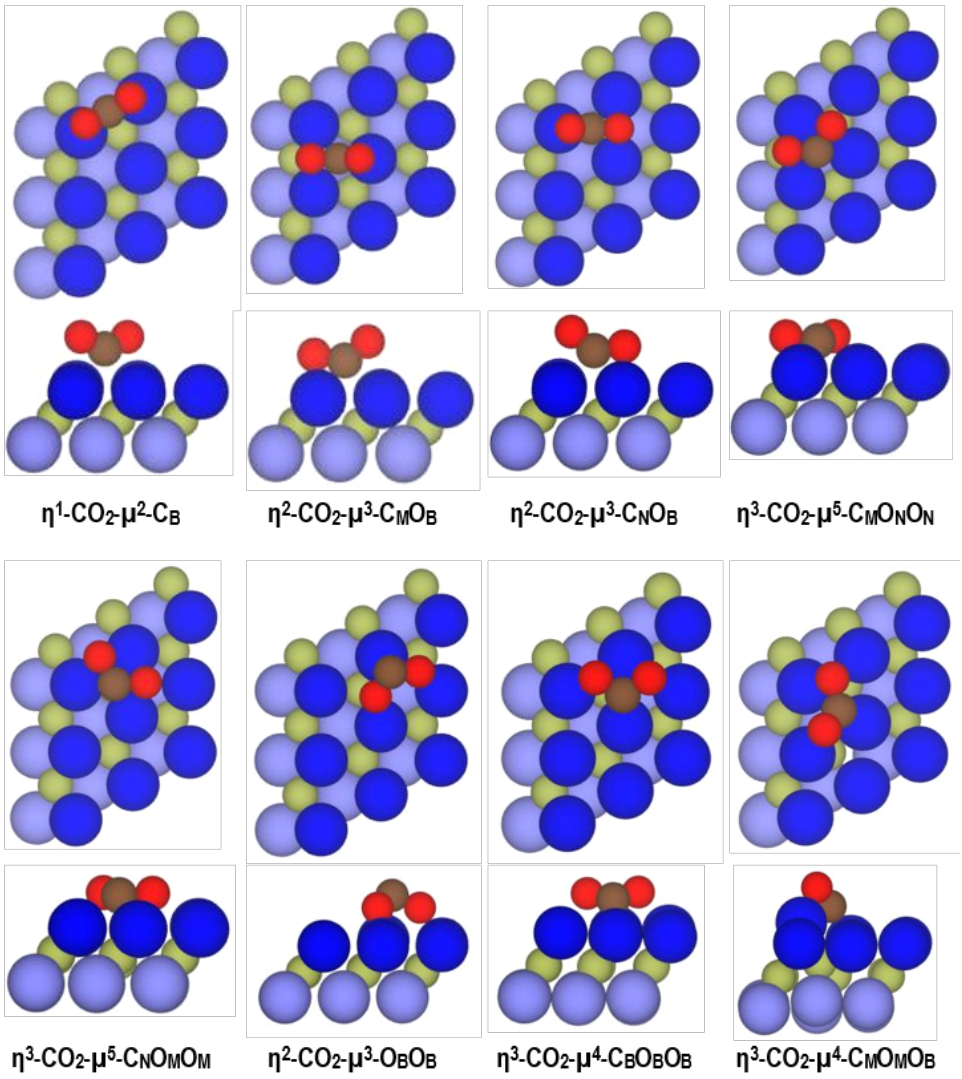

Fig. 2 (a) Adsorption and desorption rates for CO_2 interacting with the Cr_2N and Ti_2N (0001) surfaces. The points with T_1–T_6 marked labels for Cr_2N show the range of desorption temperature represented in (b). Green, gray and blue colours correspond to adsorption rates on a single site per time unit for a CO_2 partial pressure of 40, $15 \cdot 10^3$, and 10^5 Pa, respectively. Note that the bars in (b) have the same sequence of colours. Black and red lines are desorption rates per site for E_{ads} obtained from PBE (solid) and PBE-D3 (dashed) calculations.

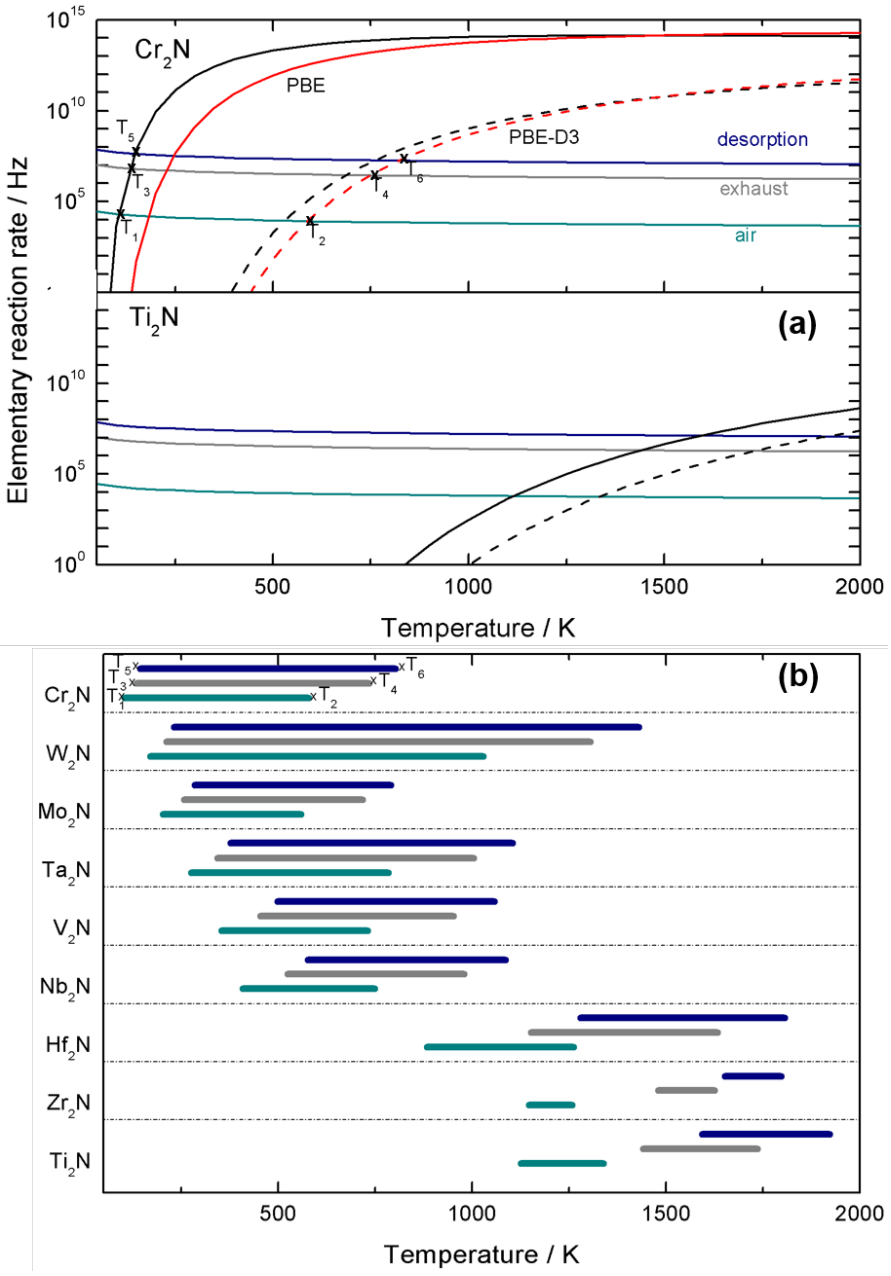

Fig. 3 Predicted CO_2 uptake by M_2N materials compared to values in the literature for zeolites (Ca-X and 13X), derivatives of graphene (a-RGO-950) and bulk MgO nanopowders is represented by dark blue, red, light blue, and dark yellow bars, respectively. Details are given in the ESI†.

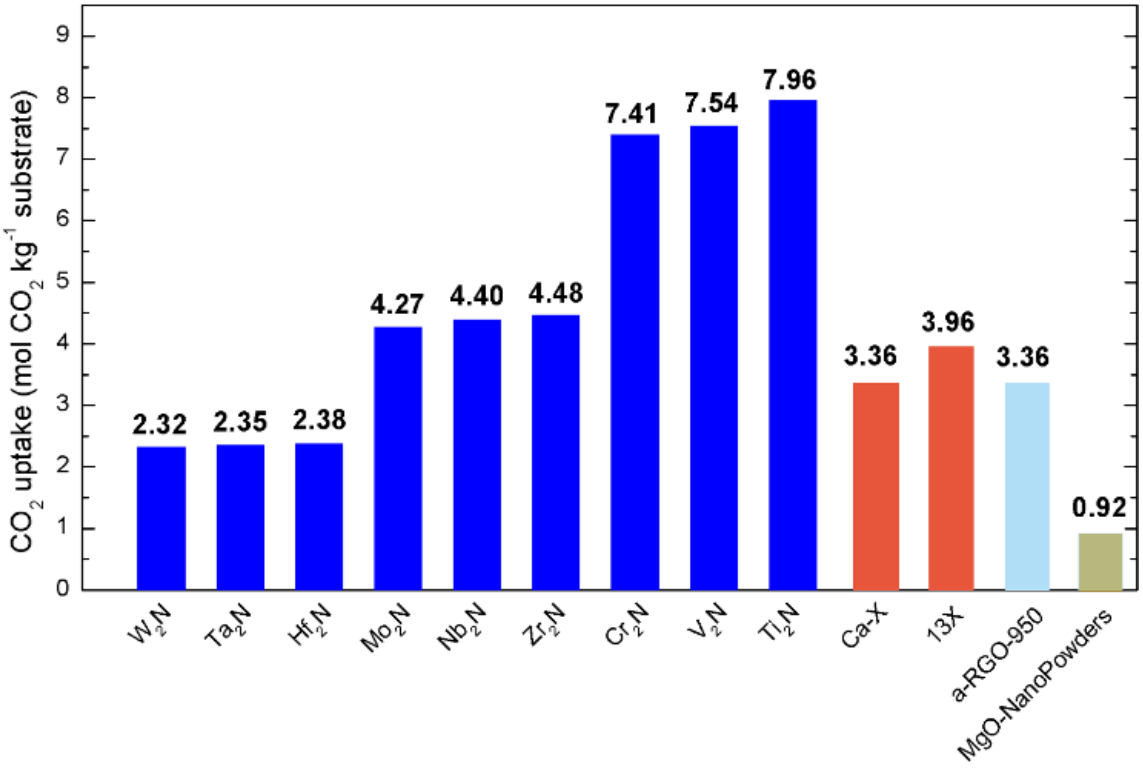

REFERENCES

(1) L. Marini, *Geological Sequestration of Carbon Dioxide, Developments in Geochemistry*, Elsevier, 2007.

(2) G. A. Olah, G. K. S. Prakash, A. Goeppert, *J. Am. Chem. Soc.,* 2011, **133**, 12881-12898.

(3) A. Goeppert, M. Czaun, G. K. S. Prakash, G. A. Olah, *Energy Environ. Sci.,* 2012, **5**, 7833-7853.

(4) U. Burghaus, *New and Future Developments in Catalysis: Activation of Carbon Dioxide*, Elsevier, 2013.

(5) A. B. Rao, E. S. Rubin, *Environ. Sci. Technol.,* 2002, **36**, 4467-4475.

(6) D. P. Hanak, E. J. Anthony, V. Manovic, *Energy Environ. Sci.,* 2015, **8**, 2199-2249.

(7) J. Kou, L.-B. Sun, *J. Mater. Chem., A* 2016, **4**, 17299-17307.

(8) D. Qian, C. Lei, E.-M. Wang, W. C. Li, A. H. Lu, *ChemSusChem,* 2014, **7**, 291-298.

(9) Y. Li, S: H. Chan, Q. Sun, *Nanoscale,* 2015, **7**, 8663-8683.

(10) P. B. Keleman, J. Matter, *Proc. Natl. Am. Soc.,* 2008, **105**, 17295-17300.

(11) E. Eikeland, A. B. Blichfeld, C. Tyrsted, A. Jensen, B. B. Iversen, *ACS Appl. Mater. Interfaces,* 2015, **7**, 5258-5264.

(12) V. A. de la Peña O´ Shea, S. González, F. Illas, J. L. G. Fierro, *Chem. Phys. Lett.,* 2008, **454**, 262-268.

(13) D. C. Sorescu, J. Lee, W. A. Al-Saidi, K. D. Jordan, *J. Chem. Phys.,* 2012, **137**, 074704:1-16.

(14) Y. Jiao, A. Du, Z. Zhu, V. Rudolph, G. Q. Lu, S. C. Smith, *Catal. Today,* 2011, **175**, 271-275.

(15) D. Smykowski, B. Szyia, J. Szczygiel, *J. Mol. Graphics Modell.,* 2013, **41**, 89-96.

(16) C. A. Trickett, A. Helal, B. A. Al-Maythalony, Z. H. Yamani, K. E. Cordova, O. M. Yaghi, *Nat. Rev. Mater.,* 2017, **2**, 17045:1-16.

(17) M. Wriedt, J. P. Sculley, A. A. Yakovenko, Y. Ma, G. J. Halder, P. B. Balbuena, H.-C. Zhou, *Angew. Chem. Int. Ed.,* 2012, **51**, 9804-9808.

(18) C. Kunkel, F. Viñes, F. Illas, *Energy Environ. Sci.,* 2016, **9**, 141-144.

(19) G. A. Mutch, S. Shulda, A. J. McCue, M. J. Menart, C. V. Ciobanu, C. Ngo, J. A. Anderson, R. M. Richards, D. Vega-Maza, *J. Am. Chem. Soc.,* 2018, **140**, 4736-4742.

(20) B. Anasori, M. R. Lukatskava, Y. Gogotsi, *Nat. Rev. Mater.,* 2017, **2**, 16098:1-17.

(21) F. Liu, A. Zhou, J. Chen, J. Cao, L. Wang, Q. Hu, *Adsorption,* 2016, **22**, 915-922.

(22) J. Zhu, E. Ha, G. L. Zhao, Y. Zhou, D. S. Huang, G. Z. Yue, L. S. Hu, N. Sun, Y. Wang, L. Y. S. Lee, C. Xu, K. Y. Wong, D. Astruc, P. X. Zhao, *Coord. Chem. Rev.,* 2017, **352**, 306-327.

(23) M. Naguib, O. Mashtalir, J. Carle, V. Presser, J. Lu, L. Hultman, Y. Gogotsi, *ACS Nano* 2012, **6**, 1322-1331.

(24) X. Yu, X. Cai, H. Cui, S.-W. Lee, X.-F. Yu, B. Liu, *Nanoscale,* 2017, **9**, 17859-17864.

(25) T. Li, L. Yao, Q. Liu, J. Gu, R. Luo, J. Li, X. Yan, W. Wang, P. Liu, B. Chen, W. Zhang, W. Abbas, R. Naz, D. Zhang, *Angew. Chem. Int. Ed.,* 2018, DOI: 10.1002/anie.201800887

(26) M. Alhabeb, K. Maleski, T. S. Mathis, A. Sarycheva, C. B. Hatter, S. Uzun, A. Levitt, Y. Gogotsi, *Angew. Chem. Int. Ed.,* 2018, DOI: 10.1002/anie.201802232

(27) A. Morales-García, A. Fernández-Fernández, F. Viñes, F. Illas, *J. Mater. Chem. A,* 2018, **6**, 3381-3385.

(28) T.-H. Bae, M. R. Hudson, J. A. Mason, W. L. Queen, J. J. Dutton, K. Sumida, K. J. Micklash, S. S. Kaye, C. M. Brown, J. R. Long, *Energy Environ. Sci.,* 2013, **6**, 128-138.

(29) C. Chen, D.-W. Park, W.-S. Ahn, *Appl. Surf. Sci.,* 2014, **292**, 63-67.

(30) S. Chowdhury, R. Balasubramanian, *Ind. Eng. Chem. Res.,* 2016, ***55***, 7906-7916.

(31) W. Gao, T. Zhou, B. Louis, Q. Wang, *Catalysts,* 2017, **7**, 116:1-15.

(32) B. Soundiraraiu, B. K. George, *ACS Nano,* 2017, **11**, 8892-8900.

(33) P. Hohenberg, W. Kohn, *Phys. Rev.,* 1964, **136**, B864-B871.

(34) W. Kohn, J. Sham, *Phys. Rev.,* 1965, **140**, A1133-A1138.

(35) J. P. Perdew, K. Burke, M. Ernzerhof, *Phys. Rev. Lett.,* 1996, **77**, 3865-3868.

(36) S. Grimme, J. Anthony, S. Ehrlich, H. A. Krieg, *J. Chem. Phys.,* 2010, **132**, 154104:1-19.

(37) P. E. Blochl, *Phys. Rev. B,* 1994, **50**, 17953-17979.

(38) H. J. Monkhrost, J. D. Pack, *Phys. Rev. B* 1976, **13**, 5188-5192.

(39) G. Kresse, J. Furthmüller, *Phys. Rev. B,* 1996, **54**, 11169-11186.

(40) G. Kresse, J. Furthmüller, *Comput. Mater. Sci.,* 1996, **6**, 15-50.

(41) S. Pogodin, N. López, *ACS Catal.,* 2014*,* **4**, 2328-2332.

(42) T. Takahashi, S. Sutherland, A. Kozyr, *Global Ocean Surface Water Partial Pressure of CO_2 Database: Measurements Performed During 1957-2014, Environmental Science Division*, Oak Ridge National Laboratory, 2015.

(43) D. M. D´Alessandro, B. Smith, J. R. Long, *Angew. Chem. Int. Ed.,* 2010, **49**, 6058-6082.

(44) M. E. Boot-Handford, J. C. Abanades, E. J. Anthony, M. J. Blunt, S. Brandani, N. Mac Dowell, J. R. Fernández, M.-C. Ferrari, R. Gross, J. P. Hallett, R. S. Haszeldine, P. Heptonstall, A. Lyngfelt, Z. Makuch, E. Mangano, R. T. J. Porter, M. Pourkashanian, G. T. Rochelle, N. Shah, J. G. Yao, P. S. Fennell, *Energy Environ. Sci.,* 2014, **7**, 130-189.

(45) K. Reuter, *Modelling and Simulation of Heterogeneous Catalytic Reactions*, Wiley-VCH Verlag GmbH & Co., ch. 3, 2011.

(46) P. W. Atkins, P. de Paula, *Atkins´ Physical Chemistry*, Oxford University Press, 8th edn., 2006.

(47) L. M. Azofra, N. Li, D. R. MacFarlane, C. Sun, *Energy Environ. Sci.,* 2016, **9**, 2545-2549.

(48) A. Tkatchenko, M. Scheffler, *Phys. Rev. Lett.,* 2009, **102**, 073005:1-4.

(49) A. Tkatchenko, R. A. DiStasio, M. Scheffler, *Phys. Rev. Lett.,* 2012, **108**, 236402:1-5.

(50) R. F. W. Bader, *Acc. Chem. Res.,* 1985, **18**, 9-15.

(51) L. E. Toth, *Transition Metal Carbides and Nitrides*, Academic Press, NY, 1971.

(52) Y. Zhong, X. Xia, F. Shi, J. Zhan, J. Tu, H. J. Fan, *Adv. Sci.,* 2016, **3**, 1500286:1-28.

(53) N. Li, X. Chen, W.-J. Ong, D. R. MacFarlane, X. Zhao, A. K. Cheetham, C. Sun. *ACS Nano,* 2017, **11**, 10825-10833.

(54) C. Kunkel, F. Viñes, F. Illas, *ACS Appl. Energy Mater.,* 2018, **1**, 43-47.

Graphic for TOC